Analyst

PAPER

View Article Online
View Journal | View Issue

Cite this: *Analyst*, 2019, **144**, 2393

Near-infrared fluorescent aza-BODIPY dyes for sensing and imaging of pH from the neutral to highly alkaline range†

Christoph Staudinger, Johanna Breininger, Ingo Klimant and Sergey M. Borisov *

Received 18th January 2019,
Accepted 4th February 2019

DOI: 10.1039/c9an00118b

rsc.li/analyst

New aza-BODIPY pH indicators with spectral properties modulated solely by photoinduced electron transfer (PET) are presented. The pH sensitive hydroxyl group is located in the *meta*-position of a phenyl substituent with respect to the aza-BODIPY core, which eliminates the conjugation to the chromophore. The new dyes show reversible "on"–"off" fluorescence response upon deprotonation of the receptor but no changes in the absorption spectrum, which is in contrast to state-of-the-art indicators of the aza-BODIPY family. This eliminates potential changes in the efficiency of the inner filter effect and Förster resonance energy transfer (FRET) and makes the new dyes suitable acceptors in light harvesting systems used for ratiometric pH imaging. The introduction of electron-withdrawing or electron-donating groups into the receptor results in a set of indicators suitable for measurements from physiological (pH 7) to very alkaline (pH 13) conditions. The new sensors are particularly promising for monitoring of pH changes in concrete, as was recently shown elsewhere.

1. Introduction

pH is one of the most important parameters in many applications[1] (*e.g.* chemical industry, biotechnology[2] and seawater measurements[3,4]). Although the pH electrode remains the most commonly used measurement device, optical pH sensor materials have been receiving increasing attention in the last few years. They can be deployed as inexpensive single-use sensors,[2] can be read out remotely with optical fibers, they are not influenced by electromagnetic interferences and can be manufactured in a wide variety of formats. For instance, optical pH sensors are available as larger sensor films for imaging,[5–7] as small spots integrated in microfluidic devices[8–12] or in microtiter plates,[13] on tapered fibers with only 8–140 μm tip diameter[14,15] or in the form of nanoparticles.[16,17]

Materials utilized for optical pH sensing include fluorescent indicators belonging to different chromophore classes (fluoresceins,[18] rhodamines,[19,20] perylenes,[21,22] 1,4-diketo-pyrrolo-pyrroles,[23] HPTS,[24,25] BODIPYs[26–30] and aza-BODIPYs).[3,29,31–35] Most of these dyes respond to pH changes in the near neutral and acidic ranges, enabling numerous applications in biology, medicine, environmental monitoring and biotechnology. In contrast, fluorescent indicators responding under alkaline conditions are comparably rare.[22,36–38] Notably, sensing in the alkaline range is of primary interest in such fields as the paper industry, waste water treatment, leather processing, and metal mining and finishing, and during microbial production involving alkaliphiles.[37] It is also of utmost importance for corrosion prediction and detection in steel-reinforced concrete structures, since the lifetime of these materials strongly depends on the internal pH. Whereas the pH values in concrete typically vary from 12.5 to 13.5 in the initial period, the medium becomes less alkaline with time but should stay above 10 to enable passivation of the steel components.[38] Here durable and low-cost materials for pH sensing are of the highest interest.[39,40]

Reported fluorescent sensors for the alkaline range possess several limitations such as comparably short absorption and emission wavelengths in the case of coumarin[38] and BODIPY[36,37] chromophores and high hydrophobicity in the case of perylene dyes.[22] Tetraaryl-aza-BODIPYs represent a particularly interesting class of fluorescent dyes showing absorption and emission in the red/NIR part of the spectrum, high molar absorption coefficients and extreme photostability.[3,31] The applications of these dyes go well beyond classical sensing and imaging[34,41,42] and include photothermal[43] and photodynamic[44] tumor therapy, photoacoustic imaging[45–47] and energy conversion.[48,49] With respect to optical pH sensing, aza-BODIPYs based on aromatic amines responding to pH under acidic conditions[33] and those based on substituted phenols with a broader range of available pK_a values[31] have

Institute of Analytical Chemistry and Food Chemistry, Graz University of Technology, Stremayrgasse 9, 8010 Graz, Austria. E-mail: sergey.borisov@tugraz.at

†Electronic supplementary information (ESI) available. See DOI: 10.1039/c9an00118b

been reported. Importantly, deprotonation of the phenol receptor (or the amine) in the *para*-position with respect to the aza-BODIPY core not only results in fluorescence quenching due to acceptor-excited photoinduced electron transfer (PET)[50] but also it is accompanied by a strong bathochromic shift of the absorption spectrum indicating additional intramolecular charge transfer (ICT) mechanisms.[3] Although such behavior is usually not critical for most applications, it definitely results in a more complex sensor behavior. First, the pH dependent absorption of the indicators affects the magnitude of the inner filter effect which depends on the dye concentration and the thickness of the sensor foil. Second, in a multi-component system (consisting, *e.g.*, of a pH indicator and a reference dye), both luminescence enhancement of the second component (due to lower absorption of the indicator at the excitation wavelength) and luminescence quenching (due to the inner-filter effect caused by the deprotonated form of the indicator) are possible. Third, since the absorption spectrum of the non-emissive deprotonated form of the indicator shows very good overlap with the emission spectrum of the protonated form and the concentration of the indicator in the sensor is fairly high (1–5 mM), quenching *via* Förster resonance energy transfer (FRET) is favored. Evidently, purely PET-based dyes make it possible to overcome the above limitations. Moreover, they would be attractive for application in light-harvesting systems for overcoming the limitation of the small Stokes shifts, typical of fluorescent dyes. For the latter, excitation at the maximum of the absorption band is virtually impossible since the excitation and emission light cannot be fully separated. In the light-harvesting system, excitation is performed at the absorption maximum of the energy donor with subsequent energy transfer to the acceptor. This allows the utilization of the high molar absorption coefficients of the donor and results in large effective Stokes shifts. The enhancement of the sensor brightness allows the production of thinner sensing layers with faster response times.

Herein we present 5 new aza-BODIPY pH indicator dyes which are decorated with a hydroxyl group in the *meta*-position of an aryl substituent. This receptor group is responsible for fluorescence quenching *via* the PET effect but neither induces the pH dependency of the absorption spectra nor negatively affects the fluorescence quantum yields. Due to electronic separation of the OH group from the electron-withdrawing core, the new dyes feature significantly higher pK_a values compared to the state-of-the-art aza-BODIPY indicators and cover the pH range from ~7 to 13. One of the indicators almost ideally matches the physiologically relevant conditions and the pH of seawater, whereas the other representatives are attractive for monitoring pH in concrete[39,40,51] and studies of alkaliphilic bacteria.[52]

2. Experimental

2.1 Materials

4′-Butoxyactophenone, 3-hydroxybenzaldehyde, 4′-methoxyacetophenone, diisopropylethylamine (DIPEA), benzaldehyde, 3-hydroxy-4-methoxybenzaldehyde, and boron trifluoride diethyl etherate were purchased from TCI Europe (http://www.tcichemicals.com). 4′-Hydroxychalcone and 4-methoxybenzaldehyde were bought from ABCR (http://www.abcr.de). 2,4-Dichloro-3-hydroxybenzaldehyde and 2,6-difluoro-3-hydroxybenzaldehyde were obtained from Fluorochem (http://www.fluorochem.co.uk). 2-Chloro-3-hydroxybenzaldehyde, nitromethane, ammonium acetate, potassium carbonate, trifluoroacetic acid and anhydrous sodium sulfate were purchased from Sigma Aldrich (http://www.sigmaaldrich.com). Deuterated chloroform ($CDCl_3$) was obtained from Euriso-top (http://www.eurisotop.com). All other solvents (reagent grade for synthesis, and analytical grade for spectroscopic measurements): tetrahydrofuran (THF), ethanol (EtOH) and cyclohexane (CH) as well as sodium chloride, potassium persulfate and the buffer salts (tris(hydroxymethyl)aminomethane (TRIS), bis(2-hydroxyethyl)amino-tris(hydroxymethyl)methane (BIS-TRIS), 2-morpholin-4-ylethanesulfonic acid (MES), 2-(cyclohexylamino)ethanesulfonic acid (CHES), 3-(cyclohexylamino)-1-propanesulfonic acid (CAPS) and sodium dihydrogen phosphate were purchased from Carl Roth (http://www.roth.de). Silica-gel (0.04–0.063 mm) and aluminium oxide were bought from Acros (http://www.fishersci.com). Polyurethane hydrogel (Hydromed D4) was purchased from AdvanSource Biomaterials (http://www.advbiomaterials.com). The poly(ethylene glycol terephthalate) (PET) support was from Pütz (http://www.puetz-folien.com). 5,5-Difluoro-1,3,7,9-tetraphenyl-5*H*-4λ^4,5λ^4-dipyrrolo[1,2-*c*:2′,1′-*f*][1,3,5,2]triazaborinine (tetraphenyl aza-BODIPY), 4-(5,5-difluoro-7-(4-hydroxyphenyl)-1,9-diphenyl-5*H*-4λ^4,5λ^4-dipyrrolo[1,2-*c*:2′,1′-*f*][1,3,5,2]triazaborinin-3-yl)-*N*-dodecylbenzamide (hydroxy dodecylamide aza-BODIPY), 3,7-bis(4-butoxyphenyl)-5,5-difluoro-1,9-diphenyl-5*H*-4λ^4,5λ^4-dipyrrolo[1,2-*c*:2′,1′-*f*][1,3,5,2]triazaborinine (dibutoxy aza-BODIPY) and 1-(4-butoxyphenyl)-4-nitro-3-phenylbutan-1-one (**d$_3$**) were prepared according to the literature procedures.[3]

2.2 Methods

Buffers with concentrations of 100 mM and pH values ranging from 5 to 13 were prepared using piperazine, MES, bis-TRIS, TRIS, CHES or CAPS. The pH, adjusted by adding 1 M HCl or 1 M NaOH aqueous solution, was controlled using a SevenEasy™ pH meter (Mettler Toledo, http://www.mt.com) equipped with a glass electrode (SenTix® HW, WTW, http://www.wtw.com). The pH meter was calibrated using standard buffer solutions with pH values of 4.01, 7.01 and 10.01 (Hanna Instruments, http://www.hannainstruments.at). The ionic strength of the buffers was set to 100 mM with NaCl as the background electrolyte. The NMR spectra were recorded on a 300 MHz instrument (Bruker) in $CDCl_3$ with tetramethylsilane (TMS) as a standard. MALDI-TOF mass spectra were recorded on a Micromass TofSpec 2E instrument in the reflectron mode at an accelerating voltage of +20 kV.

Absorption measurements were performed using a Cary 50 UV-VIS spectrophotometer from Varian, Palo Alto, USA (http://www.varianinc.com). Emission and excitation spectra were recorded on a Fluorolog® 3 Spectrofluorometer from Horiba

Scientific (http://www.horiba.com) equipped with an R2658 photomultiplier tube from Hamamatsu (http://www.hamamatsu.com) or on an F-7000 fluorescence spectrophotometer from Hitachi (http://www.hitachi-hightech.com). 100-OS precision cuvettes from Hellma Analytics with a light path of 10 mm were used (http://www.hellma-analytics.com). The fluorescence quantum yields were determined relative to dibutoxy aza-BODIPY dye (Φ = 36% in chloroform).[53]

The pH sensing behavior of the dyes was investigated by diluting a THF stock solution (0.5 mg mL^{-1}) with EtOH and subsequently mixing the resulting solution with a buffer in a ratio of 1 : 1. The concentration of the dyes in the final solution was ~1.5 × 10^{-6} M. The pH response of the dyes physically entrapped in hydrogel D4 was investigated in glass cuvettes (1 cm path length) with the foils positioned diagonally. The cuvettes were filled with buffers and washed with water after each pH buffer change.

The pH sensors utilizing the Dual Lifetime Referencing (DLR) technique were read out using a Firesting compact phase fluorometer from Pyroscience GmbH (http://www.pyroscience.com) and the measurement set-up described previously.[54] The planar foils were cut into circles and mounted on the distal end of a 1 m plastic optical fiber (Ratioplast, http://www.ratioplast.com) with the help of a home-made adaptor. The modulation frequency, LED intensity and integration time were set at 3 kHz, 80% and 16 ms, respectively. The sensors were submerged in a buffer containing 10 mM phosphate and 2 mM borate with an ionic strength of approximately 150 mM (adjusted by the addition of sodium chloride). The pH of the solution was adjusted between 5 and 12 (with steps of 0.4 pH units) by the addition of hydrochloric acid and sodium hydroxide (both 300 mM).

The imaging experiments were conducted using an AD-130GE RGB + NIR camera from JAI (http://www.jai.com). A high power yellow LED array with 12 LEDs ("12× OSRAM Oslon SSL 80 gelb Rund-Platine") with a passive cooler and a lens array with an emission angle of 30° (all obtained from LED-Tech.de Optoelectronics (http://www.led-tech.de)) was used as the excitation source. A combination of emission filters (a foil filter ("026 bright red") from LEE filters (http://www.leefilters.com) and an RG640 glass filter from Hoya (http://www.hoyafilter.com)) was mounted in front of the camera lens. The sensor material was glued to the bottom of a plastic Petri dish and submerged in the buffers during the measurements. The measurement times were 2000 ms and 600 ms for the RGB and NIR channels, respectively. The images were recorded with 12 bit color depth per channel.

Calibration curves and apparent pK_a values were obtained by fitting the plot of fluorescence intensity *vs.* pH with the Boltzmann sigmoid:

$$I = \text{Bottom} + \frac{\text{Top} - \text{Bottom}}{1 + 10^{\frac{\text{pH} - \text{p}K_a}{\text{slope}}}} \quad (1)$$

where I is the fluorescence intensity, and Bottom and Top are the lower and upper limits of the fluorescence intensity, respectively. pK_a is the apparent pK_a value and slope describes the slope at the point of inflection.

2.3 Sensor foil preparation

Sensor foils were prepared *via* knife-coating the "cocktail" containing Hydromed D4 (10 wt% with respect to the solvent) and dye (0.2 wt% with respect to the polymer) in THF on the PET support. Spacers of 1 Mil (25 μm) or 3 Mil (76 μm) were used, resulting in ~3 and 8 μm thick sensing layers after solvent evaporation. DLR referenced sensors were prepared by additionally adding microcrystalline powder of Egyptian blue[55] (40 wt% with respect to the hydrogel).

2.4 Synthesis

The synthetic procedures for the intermediates and NMR and MS spectra of the indicators can be found in the ESI (Fig. S6–S18†).

3-(3,7,9-Tris(4-butoxyphenyl)-5,5-difluoro-5*H*-5λ^4,6λ^4-dipyrrolo[1,2-*c*:2′,1′-*f*][1,3,5,2]triazaborinin-1-yl)phenol (indicator 1). 44.6 mg **e$_1$** (65.41 μmol, 1.00 eq.) were dissolved in dry DCM under an argon atmosphere in a Schlenk flask. 230 μL *N*,*N*-diisopropylethylamine (1.32 mmol, 20.19 eq.) and 160 μL boron trifluoride diethyl etherate (1.30 mmol, 19.82 eq.) were added dropwise. The solution was stirred at room temperature for 3 h during which the solution turned grey-blue. After a quantitative conversion of the ligand into the complex (monitored by TLC; DCM : CH 3 : 1), the solution was partitioned between DCM and aqueous $NaHCO_3$ solution (3 × 25 mL) and dried over sodium sulfate. The solvent was removed under reduced pressure. The crude product was purified by column chromatography (silica-gel, DCM : CH 3 : 1, detection by TLC with DCM : CH 3 : 1 and UV/VIS spectroscopy) and recrystallization from MeOH to yield red-purple crystals.

Yield: 26.1 mg (55%).

MS (MALDI): 729.3868 (calculated: 729.3557).

^{1}H NMR (300 MHz, chloroform-d): δ = 8.04 (t, J = 7.9 Hz, 6H), 7.61 (s, 1H), 7.50 (d, J = 7.5 Hz, 1H), 7.30 (d, J = 7.8 Hz, 1H), 7.06–6.90 (m, J = 8.0 Hz, 8H), 6.86 (d, J = 7.4 Hz, 1H), 5.06 (s, 1H), 4.13–3.90 (m, 6H), 1.88–1.70 (m, 6H), 1.51 (dd, J = 14.9, 7.4 Hz, 6H), 0.99 (t, J = 7.3 Hz, 9H).

^{13}C APT NMR (76 MHz, chloroform-d): δ = 161.83, 161.44, 160.73, 159.26, 156.72, 155.91, 145.83, 144.78, 143.58, 141.34, 134.28, 131.83, 131.54, 131.01, 129.76, 125.12, 124.23, 123.94, 121.49, 118.24, 117.44, 116.42, 116.01, 114.83, 77.16, 67.97, 31.35, 19.38, 13.98.

2-Chloro-3-(3,7,9-tris(4-butoxyphenyl)-5,5-difluoro-5*H*-5λ^4,6λ^4-dipyrrolo[1,2-*c*:2′,1′-*f*][1,3,5,2]triazaborinin-1-yl)phenol (indicator 2). Indicator **2** was prepared analogously to indicator **1** from 62.0 mg **e$_2$** (68.55 μmol).

Yield: 25.8 mg (39%), red crystals.

MS (MALDI): 763.2911 (calculated: 763.3168).

^{1}H NMR (300 MHz, chloroform-d): δ = 8.19–7.98 (m, J = 18.0, 8.9 Hz, 6H), 7.39–7.28 (m, J = 13.0, 6.9 Hz, 2H), 7.17–7.07 (m, 2H), 7.05–6.93 (m, 5H), 6.87 (d, J = 8.7 Hz, 2H), 5.84 (s, 1H), 4.03 (dt, J = 12.5, 6.3 Hz, 6H), 1.88–1.71 (m, J = 7.8, 5.7 Hz, 6H), 1.57–1.47 (m, J = 15.0, 7.5 Hz, 6H), 1.00 (t, J = 7.3 Hz, 9H).

^{13}C APT NMR (76 MHz, chloroform-d): δ = 162.06, 161.42, 160.80, 160.40, 155.51, 152.15, 146.41, 144.96, 144.00, 138.75, 132.20, 131.97, 131.60, 130.85, 127.23, 125.77, 124.80, 124.27, 123.82, 121.77, 119.60, 117.60, 116.11, 114.84, 77.16, 67.96, 31.37, 19.38, 13.97.

2,6-Dichloro-3-(5,5-difluoro-3,7,9-tris(4-methoxyphenyl)-5*H*-5λ^4,6λ^4-dipyrrolo[1,2-*c*:2′,1′-*f*][1,3,5,2]triazaborinin-1-yl)phenol (indicator 3). Indicator **3** was prepared analogously to indicator **1** from 60.2 mg $\mathbf{e_3}$ (96.39 μmol).

Yield: 41.3 mg (63%), green crystals.

MS (MALDI): 671.1675 (calculated: 671.1368).

^{1}H NMR (300 MHz, chloroform-d): δ = 8.20–7.95 (m, 6H), 7.35 (d, J = 5.7 Hz, 2H), 7.15 (s, 1H), 7.08–6.97 (m, J = 10.8, 4.0 Hz, 5H), 6.91 (d, J = 8.4 Hz, 2H), 3.89 (d, J = 3.2 Hz, 9H).

3-(5,5-Difluoro-3,7,9-tris(4-methoxyphenyl)-5*H*-5λ^4,6λ^4-dipyrrolo[1,2-*c*:2′,1′-*f*][1,3,5,2]triazaborinin-1-yl)-2,4-difluorophenol (indicator 4). Indicator **4** was prepared analogously to indicator **1** from 64.7 mg $\mathbf{e_4}$ (109.4 μmol).

Yield: 36.9 mg (53%), purple metallic crystals.

MS (MALDI): 639.1469 (calculated: 639.1959).

^{1}H NMR (300 MHz, chloroform-d): δ = 8.16–7.97 (m, 6H), 7.09–6.82 (m, 10H), 3.96–3.78 (m, 9H).

^{13}C APT NMR (76 MHz, chloroform-d): δ = 162.56, 161.68, 161.44, 161.30, 155.61, 152.16, 149.69, 146.58, 146.40, 144.55, 140.68, 140.43, 132.10, 131.49, 130.89, 130.10, 124.98, 124.53, 123.97, 122.12, 118.02, 117.13, 117.01, 114.48, 114.37, 114.26, 111.47, 111.15, 77.16, 55.54.

5-(5,5-Difluoro-3,7,9-tris(4-methoxyphenyl)-5*H*-5λ^4,6λ^4-dipyrrolo[1,2-*c*:2′,1′-*f*][1,3,5,2]triazaborinin-1-yl)-2-methoxyphenol (indicator 5). Indicator **5** was prepared analogously to indicator **1** from 62.0 mg $\mathbf{e_5}$ (103.73 μmol, 1.00 eq.).

Yield: 66.4 mg (98%), purple metallic crystals.

MS (MALDI): 645.2808 (calculated: 645.2617).

^{1}H NMR (300 MHz, chloroform-d): δ = 8.17–8.00 (m, J = 8.6, 3.5 Hz, 6H), 7.79 (d, J = 1.8 Hz, 1H), 7.64 (dd, J = 8.4, 1.7 Hz, 1H), 7.49 (t, J = 7.3 Hz, 2H), 7.42 (d, J = 7.0 Hz, 1H), 7.07–6.87 (m, 7H), 5.64 (s, 1H), 4.05 (t, J = 6.4 Hz, 2H), 3.97 (s, 3H), 3.89 (s, 3H), 1.86–1.74 (m, J = 14.5, 6.6 Hz, 2H), 1.56 (s, 2H), 0.99 (t, J = 7.3 Hz, 3H).

3. Results and discussion

3.1 Synthesis

The synthesis of indicators **1–5** was conducted based on the well-known route *via* nitro-chalkones (Fig. 1).[56] Here, two different nitro-chalkones ($\mathbf{b_x}$ and $\mathbf{d_x}$) are reacted to give the unsymmetrical product ($\mathbf{e_x}$) along with two symmetrical derivatives bearing no and two pH sensing functionalities, respectively. Partly due to this reason and partly because crude nitrochalkones were used, the yield of the aimed product in the condensation reaction is typically low (5–10%). Nevertheless, it is still acceptable since both chalkones and nitrochalkones can be prepared on a large scale from inexpensive chemicals. The ligand $\mathbf{e_x}$ is converted to the corresponding BF_2 chelate (indicator $\boldsymbol{x}$) with a good yield (40–90%). The introduction of substituents into all phenyl rings improved the solubility of the dyes and simplified the chromatographic separation.

3.2 Photophysical properties of the indicators

The spectral properties of the new dyes are almost identical (Table 1, Fig. S1 of the ESI†) and are very similar to those of the reported representatives of the aza-BODIPY family (Fig. 2). The dyes show the absorption and emission maximum in the NIR part of the spectrum. The molar absorption coefficients are around 80 000 L mol^{-1} cm^{-1}, a typical value for this dye class. The fluorescence quantum yield is about 25%, except for indicator **5** whose Φ is ~2-fold lower. Fluorescence decay times show the same trend with values of ~2.6 ns for indicators **1–4** and only ~1.5 ns for indicator **5**. The most important struc-

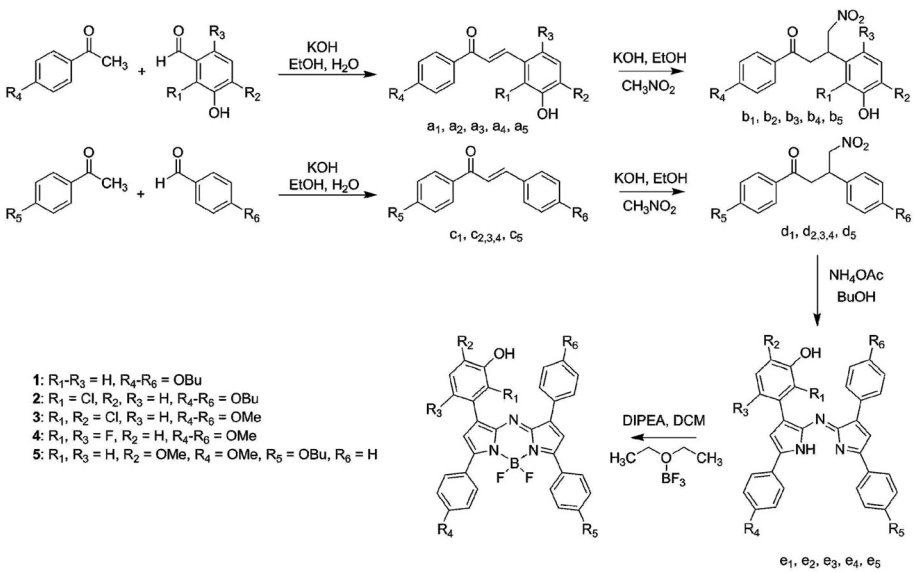

Fig. 1 Synthetic route to the new aza-BODIPY dyes. Intermediates with indices belong to the respective dye.

Table 1 Photophysical properties of the aza-BODIPY dyes in tetrahydrofuran[a]

Compound	λ_{abs}, nm	λ_{em}, nm	ε, M^{-1} cm^{-1}	Φ, %	τ, ns	pK'_a [b]	pK'_a [c]
1	696	720	83 200	24	2.54	n.d.[d]	11.7
2	696	721	85 400	27	2.69	11.1	10.8
3	695	721	80 700	26	2.56	7.8	7.5
4	694	720	73 300	27	2.67	10.3	10.3
5	698	722	90 000	14	1.57	n.d.[d]	11.6

[a] Protonated form of the dyes. [b] Determined in solution in EtOH/H_2O (1/1). [c] Determined in a Hydromed D4 sensor foil in a concentration of 0.2 w%. [d] Dye solubility is insufficient for the titration.

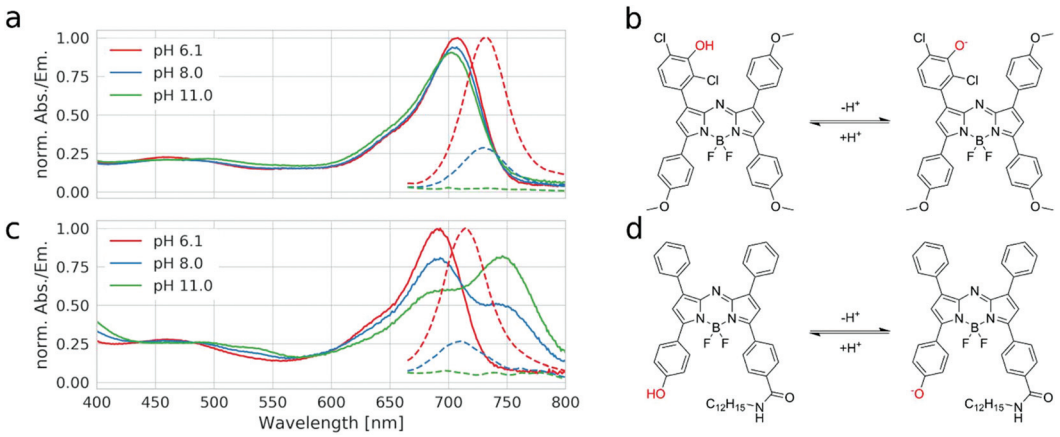

Fig. 2 pH dependence of absorption (solid lines) and emission spectra (dashed lines) of indicator **3** (a) and the state-of-the-art hydroxy-aza-BODIPY pH indicator[31] (c) in hydrogel D4; (b) and (d) show the pH equilibria for the respective dyes.

tural difference between indicators **1–4** and indicator **5** is the methoxy group in the *o*-position to the hydroxyl group. This provides the possibility of hydrogen bonding between these two groups and might cause a reduction in quantum yield and fluorescence lifetime. The brightness of the dyes is therefore significantly higher than that of the previously reported purely PET-based aza-BODIPY dye with a *meta*-hydroxyl group in the "lower" phenyl ring (Φ of 10%).[3]

3.3 pH sensing properties of the indicators and sensors

Fig. 2a exemplarily shows the pH dependency of the absorption and emission spectra for indicator **3** (the spectral changes for other indicators are almost identical). It is evident that deprotonation of the hydroxyl group has almost no effect on the absorption spectra, but it results in complete quenching of the fluorescence of the indicator. This confirms that PET is the only mechanism responsible for the spectral changes and ICT is not involved. In contrast, a state-of-the-art aza-BODIPY indicator with a hydroxyl group in the *para*-position shows an ~55 nm bathochromic shift of the absorption upon deprotonation, due to the enhancement of the ICT effect (Fig. 2c). This behavior is undesired, due to the increasing overlap between the emission of the protonated form and the absorption of the non-emissive deprotonated form of the indicator, as it promotes fluorescence quenching *via* FRET. Evidently, the new dyes overcome this drawback. The pH-independent absorption of the new dyes is particularly advantageous in the case of broad-range sensors (obtained by mixing several indicators with different pK_a values) and in multi-parameter sensors (obtained by a combination of probes for different species in one material) since undesired enhancement or quenching of the luminescence of the components due to modulation of the inner filter effect is avoided.

The fluorescence response of the new dyes to pH is typical of the "on"–"off" indicators (Fig. S2 of the ESI,† Fig. 3b). Generally, the pK_a values (Table 1) are significantly higher than those for the state-of-the-art aza-BODIPY dyes with conjugated phenol and the same substitution character. The relatively high pK_a values of the new dyes can be explained by the electronic decoupling of the hydroxyl group from the electron withdrawing core of the dye. Interestingly, the apparent pK_a for dye **1** is even higher than that for phenol (pK_a = 9.99).[57] This may be explained by the fairly hydrophobic character of the chromophore creating a microenvironment where the more polar anionic form is less stabilized than the uncharged form. Indicator **2**, which is decorated with a single chlorine atom in the *ortho*-position towards the hydroxyl group, features only a slightly lower pK_a value (Table 1). Two fluorine atoms located in the *ortho* and *para*-positions towards the hydroxyl group further decrease the pK_a value by about 1 unit. As can be seen, the effect of two chlorine atoms in the *ortho*-position towards the hydroxyl group (indicator **3**) is much stronger (pK_a = 7.8), making this indicator promising for measurements under physiological conditions in marine environment due to pK_a

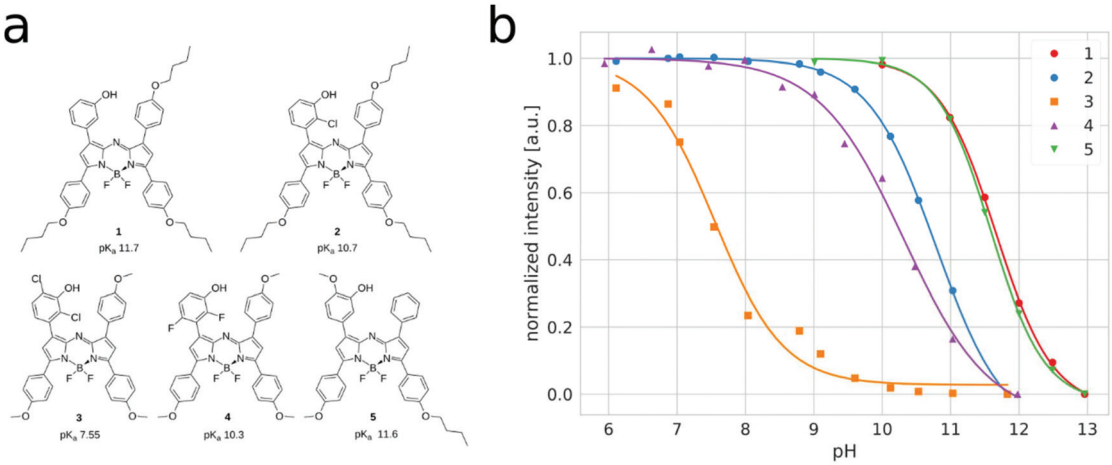

Fig. 3 Structures with apparent pK_a values (a) and titration curves (b) of the new aza-BODIPY indicators immobilized in polyurethane hydrogel D4.

almost ideally matching the pH of seawater. On the other hand, indicators **1**, **2**, **4** and **5** are expected to be promising for imaging of pH on concrete surfaces[51] and the investigation of alkaliphilic bacteria.[52] In fact, we recently demonstrated high potential of the new sensors for monitoring the pH dynamics in concrete.[39,40] The dyes can also be used as essential components for the preparation of broad range pH sensors (usually obtained by mixing multiple pH indicators).[31] Notably, only a few aza-BODIPY indicators have been reported with similarly high pK_a values and they require higher synthetic effort[31] or are no longer fluorescent and can only be used as absorption based indicators.[58]

Table 2 compares the properties of fluorescent pH indicators used in sensors for measurements in highly alkaline media. As can be seen, only BODIPYs[28] and aza-BODIPYs (this work) have so far allowed for the fine-tuning of the pK_a value and the dynamic range of the sensors. Compared to the former, the new dyes show about 150 nm bathochromically shifted absorption and emission spectra, which is beneficial for application in environments with high autofluorescence and scattering but also for *in vivo* measurements.

In order to overcome the limitations of fluorescence intensity measurement, we prepared pH sensor materials which rely on the Dual Lifetime Referencing (DLR) technique. This method relies on the use of a second emitter with a much longer luminescence decay time (micro- or millisecond time domain). It enables a robust read-out independent of the intensity of the excitation light and sensitivity of the photodetector and compensates for some variation in the thickness of the sensor foil. Similar to the previously reported aza-BODIPY indicators, the new dyes are spectrally compatible with the robust inorganic emitters Egyptian Blue[55] and Cr-GAB.[59] In fact, the sensors prepared on the basis of dyes **3** and **4** and Egyptian blue as a reference material were excellently suitable for robust referenced read-out with a compact phase fluorometer (Fig. S3 of the ESI†). The resolution of these sensors estimated from the standard deviation of the measured phase angle (~0.11°) was 0.003 pH units when measured close to the apparent pK_a of the sensors. Clearly, this referencing scheme can also be applied for the other dyes of the series.

3.4 Application of the new dyes in donor–acceptor light harvesting systems

Another application which benefits from the less complex behavior of the novel indicators is signal enhancement by light harvesting. In such a scheme a suitable antenna dye (donor) is used in a high concentration to absorb the excitation light and transfer the energy *via* FRET to the pH sensitive acceptor dye.

Table 2 Properties of pH indicators for high pH values

Dye-class	Matrix	λ_{max} abs/exc, nm	λ_{max} em, nm	pK'_a	Comment	Ref.
Coumarin	Cross-linked 1,4-bis (acryloyl)piperazine	370	470	11.9	Short wavelength absorption and emission	38
BODIPY	Polyurethane hydrogel D4	523	532	11.44	Comparably short wavelength of absorption and emission	37
BODIPY	Polymeric hydrogel	502	508	10.8	Comparably short wavelength of absorption and emission	36
BODIPY	Polyurethane hydrogel D4	522–540	537–550	0.5–12.83	Comparably short wavelength of absorption and emission	28
Perylene	Polyurethane hydrogel D4	586	595	10.56	Extremely limited tuneability of the pK_a	22
Perylene	Polyurethane hydrogel D4	650	662	10.15	Extremely limited tuneability of the pK_a	22
Aza-BODIPYs	Polyurethane hydrogel D4	694–698	720–722	7.5–11.7	Tuneable pK_a, NIR absorption and emission, high photostability; excellent spectral compatibility with robust reference materials	This work

Thereby the overall brightness of the sensor material is significantly enhanced. Such an enhancement is not possible by simply using a higher concentration of the indicator since this would lead to undesired negative effects like aggregate formation, strong inner filter effect and shift of the apparent pK_a caused by homo-FRET (energy transfer from the protonated form of the indicator to its deprotonated form). By employing an antenna dye to enhance the absorption of the sensor film the above problems can be avoided since the antenna dye cannot reabsorb the emitted fluorescence or act as a FRET acceptor for the pH sensitive dye. Moreover, this scheme enables an artificial increase of the Stokes shift of the sensor material, due to the hypsochromically shifted absorption of the antenna dye. A large Stokes shift is beneficial as excitation and emission light can be separated more easily and with lower losses. Moreover, potentially remaining antenna fluorescence can be used for ratiometric measurements.

State-of-the-art *para*-substituted-hydroxy aza-BODIPY indicators are not ideal for this concept as the efficiency of energy transfer depends on the overlap of the absorption and emission spectra of the donor and the acceptor, respectively. A strong bathochromic shift in the absorption of the acceptor upon deprotonation (see Fig. 2a) results in reduced FRET efficiency and a "turn on" effect of the donor, which reduces the dynamics of the sensor.

Fig. 4a depicts the composition of the light harvesting system which relies on the pH-insensitive tetraphenyl aza-BODIPY as an energy donor and indicator **3** as an acceptor. Importantly, the absorption spectrum of **3** is bathochromically shifted by approximately 40 nm due to the electron donating ether groups (see Fig. S4 of the ESI†), thus ensuring excellent spectral overlap between the emission of the donor and the absorption of the acceptor. The protonated indicator can indeed be efficiently excited *via* energy transfer from the donor (Fig. 4b). The corresponding emission spectra (Fig. 4c) of the materials clearly show that the light harvesting concept leads to a strong signal enhancement (~3.4 fold) of the fluorescence of the pH indicator. The energy transfer is very efficient since only a small amount of residual donor fluorescence is visible. In basic media (Fig. 4d and e), the fluorescence emission of the acceptor is completely quenched. In contrast, the residual fluorescence of the donor remains constant (Fig. 4e, peak at 690 nm). Furthermore, no "turn on" of donor emission is visible upon deprotonation of the indicator. Therefore, even a simple long-pass emission filter (*e.g.* at 700 nm) makes it possible to collect almost the entire fluorescence from the indicator. The strong signal enhancement can either be used to prepare thinner and faster responding sensor films or to obtain sensors with better signal-to-noise ratios. Additionally, the residual fluorescence from the donor is also very useful for referencing purposes.

3.5 Ratiometric imaging of the pH distribution

As was shown above, light harvesting not only enhances the brightness of the sensors but also allows the utilization of the residual fluorescence of the donor for referencing purpose.

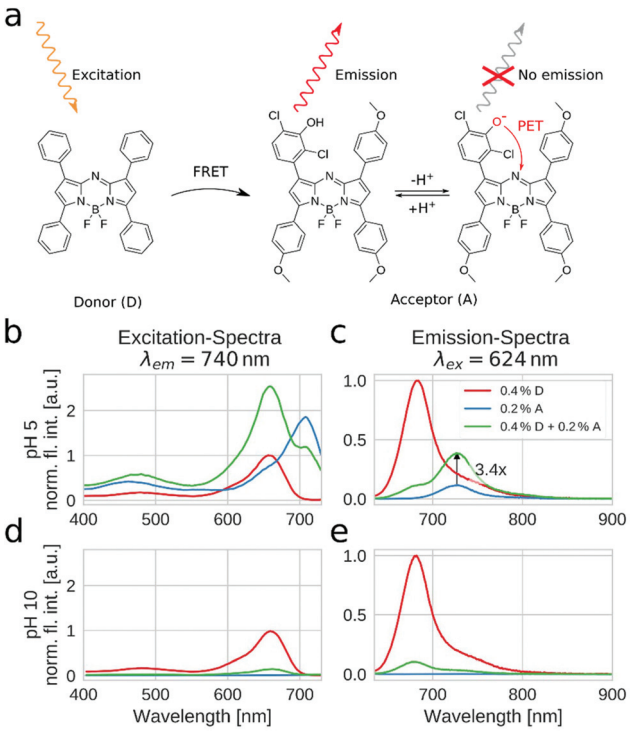

Fig. 4 Enhancement of the fluorescence properties of the pH sensor *via* light harvesting. Chemical structures of the employed donor (tetraphenyl aza-BODIPY) and acceptor (indicator **3**) (a). Excitation (b, d) and emission (c, e) spectra at pH 5 (b, c) and pH 10 (d, e) for the sensor material employing light harvesting (green) and for the corresponding sensor materials containing only the donor (red) and only the acceptor (blue). The concentrations of the dyes are given in wt% with respect to the polymer. The spectra were recorded with sensor foils of approximately 3 μm sensor layer thickness in the right angle mode. The emission intensities are normalized to the emission intensity of the pure donor for every plot. The absorption spectra of the sensor foil are depicted in Fig. S1 in the ESI.†

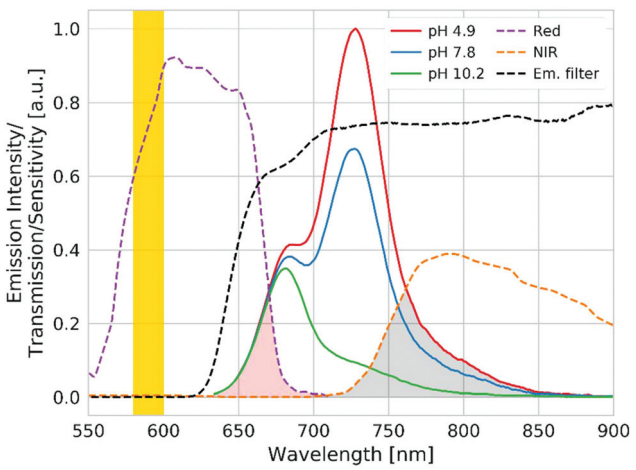

Fig. 5 pH dependency of the emission spectrum of the sensor and the optical properties of the imaging set-up. The orange vertical line indicates excitation from the high power 590 nm LED; dashed purple and orange lines show the relative sensitivity of the red and NIR channels of the camera, respectively (adapted from http://www.jai.com). The dashed black line is the transmission of the used emission filter (RG640 from Hoya combined with the "bright red" foil filter from LEE filters in the front).

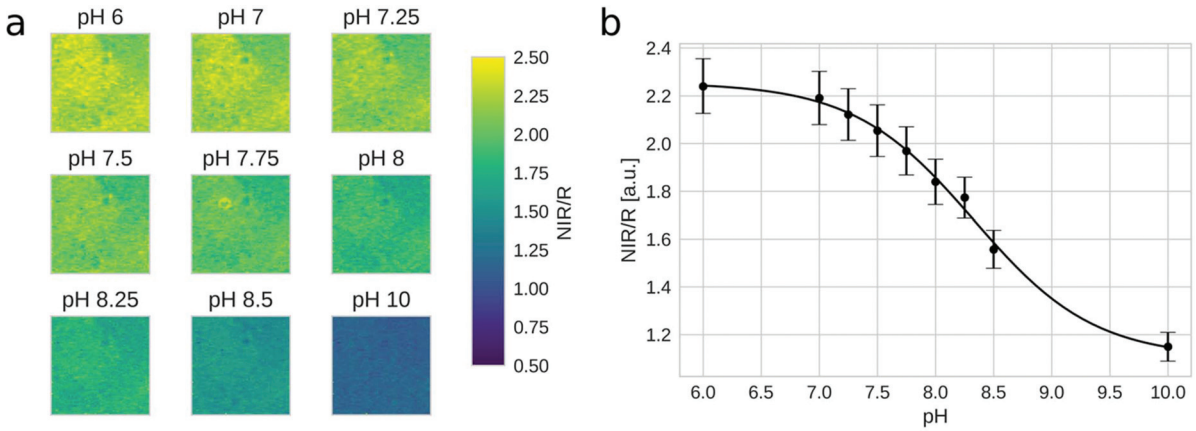

Fig. 6 Imaging of the pH distribution with the dual chip RGB/NIR camera. (a) False-color images for the fluorescence ratio (NIR/red channel) for the sensor material between pH 6 and 10. (b) The fit of the corresponding response curve with the Boltzmann sigmoid function.

Thus, ratiometric imaging of the pH distribution with an inexpensive setup becomes possible. The imaging set-up consists of a yellow high power LED and a 4-channel camera (blue, green, red and NIR channels)[5] equipped with a long-pass emission filter (Fig. S5†). Fig. 5 shows the spectral properties of the sensor material (0.4 wt% antenna dye and 0.2 wt% indicator **3**) along with the spectral sensitivity of the red and NIR channels of the camera. As can be seen, the emission of the indicator in the NIR channel is modulated by pH. On the other hand, the residual emission of the donor dye in the red channel is virtually pH independent, thus enabling ratiometric referencing. Although this set-up may not be ideal due to the fact that only a small portion of the emission of the donor and the acceptor is collected in the respective channels (Fig. 5), the camera is compact, affordable (~2000 €) and contains no moving elements. A spectral camera with custom emission filters on a rotating wheel[60] may be an interesting alternative if higher signals are desired. Nevertheless, due to strong brightness enhancement *via* light harvesting, even the current combination is promising for imaging of the pH distribution (Fig. 6a). The calibration curve generated from ratiometric images (Fig. 6b) is very similar to that obtained for the unreferenced fluorescence intensity measurements (Fig. 3). It should be mentioned here that the Dual Lifetime Referencing scheme can also be used as an alternative to the ratiometric two wavelength imaging as recently demonstrated for sensors applied for the investigation of corrosion processes in concrete.[39,40] On the other hand, the DLR sensors require much more expensive cameras operating in the time or the frequency domain, which may be a serious limitation.

4. Conclusions

In conclusion, we prepared 5 new pH-sensitive aza-BODIPY indicator dyes that feature different substitution patterns compared to the state-of-the-art analogs. The new indicators possess good quantum yields in the "on" state and no detectable fluorescence in the "off" state. They are purely PET-based, featuring nearly pH independent absorption spectra and therefore constant magnitude of the inner filter effect in sensor materials. These properties make the new dyes promising for application in multi-parameter sensors and systems utilizing signal enhancement *via* light harvesting. The apparent pK_a values between 7.5 and 11.7 enable measurements from physiological conditions to very alkaline media. Whereas the indicator bearing two chlorine atoms in the *ortho*-position ideally matches the pH of seawater, the other dyes have very high pK_a values due to the decoupling from the electron withdrawing core of the dye. The dynamic range of these sensors corresponds to typical pH changes occurring in concrete which promote corrosion and deterioration of the structures. Therefore, they are not only suitable for the detailed investigation of these processes as recently demonstrated by our group, but potentially also for long-term monitoring of concrete "heath" with low-cost optical sensors. They may also be promising for the investigation of alkaliphiles or for the design of optical CO_2 sensor materials utilizing fluorescent pH indicators as transducers.

Conflicts of interest

There are no conflicts to declare.

Acknowledgements

This work was supported by the European Union's Horizon 2020 project STEMM-CCS (grant number 654462).

References

1 D. Wencel, T. Abel and C. McDonagh, *Anal. Chem.*, 2012, **86**, 15–29.

2 E. Vachette, C. Fenge, J.-M. Cappia, L. Delaunay, G. Greller and B. Magali, *BioProcess Int.*, 2014, **12**, 23–25.
3 T. Jokic, S. M. Borisov, R. Saf, D. A. Nielsen, M. Kühl and I. Klimant, *Anal. Chem.*, 2012, **84**, 6723–6730.
4 M. Larsen, S. M. Borisov, B. Grunwald, I. Klimant and R. N. Glud, *Limnol. Oceanogr.: Methods*, 2011, **9**, 348–360.
5 J. Ehgartner, H. Wiltsche, S. M. Borisov and T. Mayr, *Analyst*, 2014, **139**, 4924–4933.
6 Z. Jiang, X. Yu and Y. Hao, *Sensors*, 2017, **17**, 1316.
7 M. Moßhammer, M. Strobl, M. Kühl, I. Klimant, S. M. Borisov and K. Koren, *ACS Sens.*, 2016, **1**, 681–687.
8 I. B. Tahirbegi, J. Ehgartner, P. Sulzer, S. Zieger, A. Kasjanow, M. Paradiso, M. Strobl, D. Bouwesa and T. Mayr, *Biosens. Bioelectron.*, 2017, **88**, 188–195.
9 P. Gruber, M. P. C. Marques, P. Sulzer, R. Wohlgemuth, T. Mayr, F. Baganz and N. Szita, *Biotechnol. J.*, 2017, **12**, 1600475.
10 E. Poehler, C. Herzog, S. A. Pfeiffer, C. Lotter, A. J. Peretzki, D. Aigner, T. Mayr, E. Beckert and S. Nagl, *Procedia Eng.*, 2015, **120**, 175–179.
11 E. B. Magnusson, S. Halldorsson, R. M. T. Fleming and K. Leosson, *Biomed. Opt. Express*, 2013, **4**, 1749–1758.
12 L. Florea, C. Fay, E. Lahiff, T. Phelan, N. E. O'Connor, B. Corcoran, D. Diamond and F. Benito-Lopez, *Lab Chip*, 2013, **13**, 1079–1085.
13 S. Wu, S. S. Wu, Z. Yi, F. Zeng, W. Wu, Y. Qiao, X. Zhao, X. Cheng and Y. Tian, *Sensors*, 2018, **18**, 564.
14 I. Kasik, J. Mrazek, T. Martan, M. Pospisilova, O. Podrazky, V. Matejec, K. Hoyerova and M. Kaminek, *Anal. Bioanal. Chem.*, 2010, **398**, 1883–1889.
15 A. S. Kocincova, S. M. Borisov, C. Krause and O. S. Wolfbeis, *Anal. Chem.*, 2007, **79**, 8486–8493.
16 S. W. Bishnoi, C. J. Rozell, C. S. Levin, M. K. Gheith, B. R. Johnson, D. H. Johnson and N. J. Halas, *Nano Lett.*, 2006, **6**, 1687–1692.
17 R. V. Benjaminsen, H. Sun, J. R. Henriksen, N. M. Christensen, K. Almdal and T. L. Andresen, *ACS Nano*, 2011, **5**, 5864–5873.
18 H. N. Kim, K. M. K. Swamy and J. Yoon, *Tetrahedron Lett.*, 2011, **52**, 2340–2343.
19 D. Aigner, S. M. Borisov, F. J. Orriach Fernández, J. F. Fernández Sánchez, R. Saf and I. Klimant, *Talanta*, 2012, **99**, 194–201.
20 Q.-J. Ma, H.-P. Li, F. Yang, J. Zhang, X.-F. Wu, Y. Bai and X.-F. Li, *Sens. Actuators, B*, 2012, **166–167**, 68–74.
21 D. Aigner, S. M. Borisov, P. Petritsch and I. Klimant, *Chem. Commun.*, 2013, **49**, 2139–2141.
22 D. Pfeifer, I. Klimant and S. M. Borisov, *Chem. – Eur. J.*, 2018, **24**, 10711–10720.
23 D. Aigner, B. Ungerböck, T. Mayr, R. Saf, I. Klimant and S. M. Borisov, *J. Mater. Chem. C*, 2013, **1**, 5685–5693.
24 H. R. Kermis, Y. Kostov and G. Rao, *Analyst*, 2003, **128**, 1181–1186.
25 D. Wencel, B. D. MacCraith and C. McDonagh, *Sens. Actuators, B*, 2009, **139**, 208–213.
26 Z. Li, L.-J. Li, T. Sun, L. Liu and Z. Xie, *Dyes Pigm.*, 2016, **128**, 165–169.
27 Y. S. Marfin, M. V. Shipalova, V. O. Kurzin, K. V. Ksenofontova, A. V. Solomonov and E. V. Rumyantsev, *J. Fluoresc.*, 2016, **26**, 2105–2112.
28 R. Gotor, P. Ashokkumar, M. Hecht, K. Keil and K. Rurack, *Anal. Chem.*, 2017, **89**, 8437–8444.
29 A. Loudet and K. Burgess, *Chem. Rev.*, 2007, **107**, 4891–4932.
30 T. C. Werner, C. Huber, S. Heinl, M. Kollmannsberger, J. Daub and O. S. Wolfbeis, *Fresenius' J. Anal. Chem.*, 1997, **359**, 150–154.
31 M. Strobl, T. Rappitsch, S. M. Borisov, T. Mayr and I. Klimant, *Analyst*, 2015, **140**, 7150–7153.
32 J. Killoran, S. O. McDonnell, J. F. Gallagher and D. F. O'Shea, *New J. Chem.*, 2008, **32**, 483–489.
33 S. O. McDonnell and D. F. O'Shea, *Org. Lett.*, 2006, **8**, 3493–3496.
34 J. Murtagh, D. O. Frimannsson and D. F. O'Shea, *Org. Lett.*, 2009, **11**, 5386–5389.
35 A. Kamkaew and K. Burgess, *Chem. Commun.*, 2015, **51**, 10664–10667.
36 T. Gareis, C. Huber, O. S. Wolfbeis and J. Daub, *Chem. Commun.*, 1997, 1717–1718.
37 M. Hecht, W. Kraus and K. Rurack, *Analyst*, 2013, **138**, 325–332.
38 T. H. Nguyen, T. Venugopala, S. Chen, T. Sun, K. T. V. Grattan, S. E. Taylor, P. A. M. Basheer and A. E. Long, *Sens. Actuators, B*, 2014, **191**, 498–507.
39 C. Grengg, C. B. Müller, C. Staudinger, F. Mittermayr, J. Breininger, B. Ungerböck, S. M. Borisov, T. Mayr and M. Dietzel, *Cem. Concr. Res.*, 2019, **116**, 231–237.
40 B. Müller, C. Grengg, V. Schallert, M. Sakoparnig, C. Staudinger, J. Breininger, F. Mittermayr, B. Ungerböck, S. Borisov, M. Dietzel and T. Mayr, *RILEM Tech. Lett.*, 2018, **3**, 39–45.
41 N. Adarsh, M. S. Krishnan and D. Ramaiah, *Anal. Chem.*, 2014, **86**, 9335–9342.
42 H. He, J. Zhang, Y. Xie, Y. Lu, J. Qi, E. Ahmad, X. Dong, W. Zhao and W. Wu, *Mol. Pharm.*, 2016, **13**, 4013–4019.
43 Y. Xu, T. Feng, T. Yang, H. Wei, H. Yang, G. Li, M. Zhao, S. Liu, W. Huang and Q. Zhao, *ACS Appl. Mater. Interfaces*, 2018, **10**, 16299–16307.
44 Y. Xu, M. Zhao, L. Zou, L. Wu, M. Xie, T. Yang, S. Liu, W. Huang and Q. Zhao, *ACS Appl. Mater. Interfaces*, 2018, **10**, 44324–44335.
45 H. Li, P. Zhang, L. P. Smaga, R. A. Hoffman and J. Chan, *J. Am. Chem. Soc.*, 2015, **137**, 15628–15631.
46 Y. Gawale, N. Adarsh, S. K. Kalva, J. Joseph, M. Pramanik, D. Ramaiah and N. Sekar, *Chem. – Eur. J.*, 2017, **23**, 6570–6578.
47 K. Miki, A. Enomoto, T. Inoue, T. Nabeshima, S. Saino, S. Shimizu, H. Matsuoka and K. Ohe, *Biomacromolecules*, 2017, **18**, 249–256.
48 T. Li, T. Meyer, R. Meerheim, M. Höppner, C. Körner, K. Vandewal, O. Zeika and K. Leoa, *J. Mater. Chem. A*, 2017, **5**, 10696–10703.

49 J. Min, T. Ameri, R. Gresser, M. Lorenz-Rothe, D. Baran, A. Troeger, V. Sgobba, K. Leo, M. Riede, D. M. Guldi and C. J. Brabec, *ACS Appl. Mater. Interfaces*, 2013, **5**, 5609–5616.
50 D. Aigner, S. A. Freunberger, M. Wilkening, R. Saf, S. M. Borisov and I. Klimant, *Anal. Chem.*, 2014, **86**, 9293–9300.
51 E. Liu, M. Ghandehari, C. Brückner, G. Khalil, J. Worlinsky, W. Jin, A. Sidelev and M. A. Hyland, *Cem. Concr. Res.*, 2017, **95**, 232–239.
52 J. L. Slonczewski, M. Fujisawa, M. Dopson and T. A. Krulwich, in *Advances in Microbial Physiology*, Elsevier, 2009, vol. 55, pp. 1–317.
53 P. W. Zach, S. A. Freunberger, I. Klimant and S. M. Borisov, *ACS Appl. Mater. Interfaces*, 2017, **9**, 38008–38023.
54 C. Staudinger, M. Strobl, J. Breininger, I. Klimant and S. M. Borisov, *Sens. Actuators, B*, 2019, **282**, 204–217.
55 S. M. Borisov, C. Würth, U. Resch-Genger and I. Klimant, *Anal. Chem.*, 2013, **85**, 9371–9377.
56 A. Gorman, J. Killoran, C. O'Shea, T. Kenna, W. M. Gallagher and D. F. O'Shea, *J. Am. Chem. Soc.*, 2004, **126**, 10619–10631.
57 Z. Rappoport, *CRC handbook of tables for organic compound identification*, CRC Press, 1967, p. 434.
58 S. Schutting, T. Jokic, M. Strobl, S. M. Borisov, D. de Beer and I. Klimant, *J. Mater. Chem. C*, 2015, **3**, 5474–5483.
59 S. M. Borisov, K. Gatterer, B. Bitschnau and I. Klimant, *J. Phys. Chem. C*, 2010, **114**, 9118–9124.
60 M. Kühl, L. Behrendt, E. Trampe, K. Qvortrup, U. Schreiber, S. M. Borisov, I. Klimant and A. W. Larkum, *Front. Microbiol.*, 2012, **3**, 402.